BEILSTEIN JOURNAL OF NANOTECHNOLOGY

# Efficient liquid exfoliation of $KP_{15}$ nanowires aided by Hansen's empirical theory

Zhaoxuan Huang[1], Zhikang Jiang[1], Nan Tian[*1], Disheng Yao[1], Fei Long[1], Yanhan Yang[2] and Danmin Liu[*3]

Full Research Paper

Open Access

Address:
[1]School of Materials Science and Engineering, Guangxi Key Laboratory of Optical and Electronic Materials and Devices, Collaborative Innovation Center for Exploration of Nonferrous Metal Deposits and Efficient Utilization of Resources, Guilin University of Technology, Guilin 541004, China, [2]School of Science, Xi'an University of Posts and Telecommunications, Xi'an 710121, China and [3]Institute of Microstructure and Property of Advanced Materials, Beijing University of Technology, Beijing, China

Email:
Nan Tian[*] - 837549356@qq.com; Danmin Liu[*] - dmliu@bjut.edu.cn

* Corresponding author

Keywords:
Hansen's empirical theory; $KP_{15}$; liquid exfoliation; nanodevices; nanowires; Raman; semiconductors

*Beilstein J. Nanotechnol.* **2022,** *13,* 788–795.
https://doi.org/10.3762/bjnano.13.69

Received: 11 May 2022
Accepted: 27 July 2022
Published: 17 August 2022

Associate Editor: S. Giordani



## Abstract

The $KP_{15}$ nanowires with one-dimensional properties has a defect-free surface, high anisotropy, and carrier mobility which is desirable for the development of novel nanodevices. However, the preparation of nanoscale $KP_{15}$ is still inefficient. In this work, the Hansen solubility parameters of $KP_{15}$ were first obtained. Based on the Hansen's empirical theory, the concentration of liquid-exfoliated $KP_{15}$ nanowires was improved to 0.0458 $mg{\cdot}mL^{-1}$ by a solution containing 50% water and 50% acetone. Approximately 79% of the $KP_{15}$ nanowires had a thickness value below 50 nm and 60.9% of them had a width value below 100 nm. The thinnest $KP_{15}$ nanowires reached 5.1 nm and had smooth boundaries. Meanwhile, strong temperature-dependent Raman response in exfoliated $KP_{15}$ nanowires has been observed, which indicates a strong phonon–phonon coupling in those nanowires. This is helpful for non-invasive temperature measurements of $KP_{15}$ nanodevices.

## Introduction

Low-dimensional materials have drawn significant attention in recent years. So far, not only new composite materials with excellent properties have been obtained by the synthesis of different materials, but also low-dimensional materials with different properties than those of bulk materials have been synthesized by physical and chemical methods. For instance, Bingjun

Yang used one-dimensional graphene nanoscroll-wrapped MnO nanoparticles as anode materials to promote the rapid diffusion and electron transfer of lithium, and Rongjun Zhao prepared *n*-butanol gas sensors with one-dimensional $In_2O_3$ nanorods [1,2]. Different from 2D materials, 1D materials generally have a chain-like crystal structure and are easily exfoliated due to a weak interaction between these chains [3,4]. Therefore, those 1D materials have defect-free surfaces, high anisotropy, and carrier mobility. For example, $TiS_3$ nanowires obtained by mechanical stripping have a large carrier mobility of about 10000 $cm^2 \cdot V^{-1} \cdot s^{-1}$ [5-7]. Fibrous phosphorus is also a new one-dimensional material with high carrier mobility (308 $cm^2 \cdot V^{-1} \cdot s^{-1}$) and rapid response time [8-10]. These one-dimensional materials are ideal for photovoltaic and photocatalytic applications.

The $KP_{15}$ is considered to be a novel low-dimensional material with layered structure, high hole carrier mobility (1000 $cm^2 \cdot V^{-1} \cdot s^{-1}$), and highly anisotropic properties [11]. The photodetectors prepared with $KP_{15}$ have a fast response time and are ideal materials for photovoltaic applications [12]. Based on our previous studies, $KP_{15}$ is also a one-dimensional material with a defect-free surface [13,14]. This is beneficial for the development of high-performance nanodevices. Searching effective synthesis routes for nanoscale $KP_{15}$ has become an urgent issue. Liquid-phase exfoliation is one of the most straightforward methods to prepare low-dimensional materials at a low cost and with simple processes and high flexibility. In this case, the surface of bulk materials is peeled off or corroded by physical or chemical reactions in a liquid medium, and finally low-dimensional materials are obtained. Based on the Hansen's empirical theory, the exfoliation efficiency of low-dimensional materials can be improved by adjusting the composition and type of solutions used in the liquid-phase exfoliation [15-17]. This theory has been successfully used for improving the exfoliation efficiency in several low-dimensional materials, such as carbon, graphene, metal oxides, and fibrous phosphorus. [18].

In a previous study, we exfoliated $KP_{15}$ in alcohol; however, this method was still inefficient [13]. Herein, the Hansen's empirical theory was firstly introduced to improve the liquid-phase exfoliation efficiency of $KP_{15}$ nanowires. In addition, Hansen solubility parameters (HSPs) for $KP_{15}$ were also obtained in this work. By using a solution containing 50% water and 50% acetone, the exfoliation efficiency of $KP_{15}$ was effectively improved. Our results show that 79% of the $KP_{15}$ nanowires had thickness values below 50 nm and 60.9% of these nanowires had width values below 100 nm. The thinnest $KP_{15}$ nanowires reached 5.1 nm and had smooth boundaries. Meanwhile, a strong temperature-dependent Raman response was found in exfoliated $KP_{15}$ nanowires. This indicates a strong phonon–phonon coupling in $KP_{15}$ nanowires, which favors non-invasive temperature measurements of $KP_{15}$ nanodevices.

# Methods

## Synthesis of $KP_{15}$ bulks

The $KP_{15}$ bulks were prepared by the gas-phase transfer method. High-purity red phosphorus (1.370 g, 99.9999%) and metallic potassium (0.130 g, 97%) were mixed in a quartz tube. The temperature gradient in the quartz tube was 650 °C/400 °C and the heat treatment time was 12 h. After annealed, dark-red $KP_{15}$ bulks were finally obtained.

## Liquid exfoliation

For the liquid-exfoliation process, 1 mg of $KP_{15}$ was mixed in 20 mL of solvent and ultrasonically processed at a power of 80 W in an ice bath for 6 h, followed by centrifugation at 2000 rpm for 20 min. For the samples with predetermined concentration, centrifugation was not used.

## Measurement equipment

UV−visible spectrophotometry was performed by using a Shimadzu UV-3101PC system. Atomic force microscopy (AFM) tests were performed in a Multimode 8 system. The Raman tests were performed on a WITec alpha300 RA confocal Raman microscopy system. For the Raman tests, $KP_{15}$ samples were spun on $SiO_2$(300 nm)/Si substrates. The excitation wavelength used was 532 nm, the spot size was approx. 1 μm, and the laser power was kept below 20 μW. For low-temperature Raman measurements, a Linkam THMS600 cryostat cooled by liquid nitrogen was used to control the temperature. To prevent sample drift, $SiO_2$ (300 nm)/Si substrates with tested $KP_{15}$ samples were attached by fixtures to the Linkam THMS600 cryostat.

# Results and Discussion

$KP_{15}$ bulks, prepared by the gas-phase-transfer method, had a flat and smooth surface shown in Figure 1a. The X-ray diffraction patterns of the synthesized $KP_{15}$ were both theoretically calculated and experimentally measured. The consistency between the two patterns shows that there is no impurity phase (Figure 1b), which confirms an excellent crystallization quality of the $KP_{15}$ bulks.

## Measurement of the absorption coefficient and the Hansen solubility parameters for $KP_{15}$

According to the Hansen's theory [19], the dispersed concentration $C$ of a $KP_{15}$ dispersion prepared by liquid exfoliation can be expressed by Equation 1 as follows.

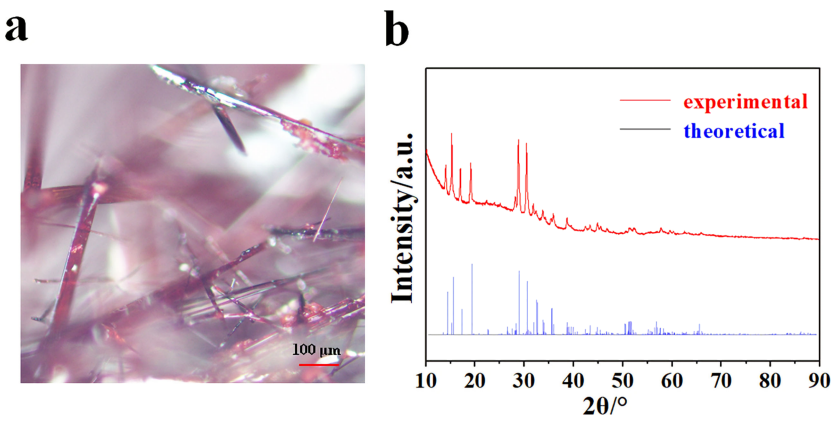


**Figure 1:** (a) Optical microscopy result of $KP_{15}$ bulks. (b) XRD results of $KP_{15}$ bulks.

$$1/C \propto \tau = \left(\delta_{A,D} - \delta_{B,D}\right)^2 + \left(\delta_{A,P} - \delta_{B,P}\right)^2/4 + \left(\delta_{A,H} - \delta_{B,H}\right)^2/4, \quad (1)$$

where $\delta_D$ is the intermolecular dispersion force, $\delta_H$ is the intermolecular hydrogen bond; $\delta_P$ is the intermolecular polar force; $\delta_{A,D}$, $\delta_{A,P}$, $\delta_{A,H}$ are the Hansen solubility parameters (HSPs) of the solute; and $\delta_{B,D}$, $\delta_{B,P}$, $\delta_{B,H}$ are the HSPs of the solvent. Therefore, to get a high concentration of $KP_{15}$ in dispersion, the HSPs of the solvent for the exfoliation of $KP_{15}$ should be close to those of $KP_{15}$. A weighted average method was used to calculate the HSPs of $KP_{15}$. The concentration of $KP_{15}$ was used as a weight factor for each suspension. This way, the HSPs of $KP_{15}$ can be expressed according to Equation 2 [19].

$$\delta_i = \frac{\sum C\delta_{i,\mathrm{sol}}}{\sum C}, \quad (2)$$

where $\delta_{i,\mathrm{sol}}$ are the HSPs of the solvent and $C$ is the concentration of the $KP_{15}$ dispersions. The Lambert–Beer law (Equation 3) was then used to measure the concentration of the $KP_{15}$ dispersions:

$$A = KbC, \quad (3)$$

where $A$ is the absorbance, $K$ is the absorption coefficient of the material, $b$ is the absorbing layer thickness (which in this work is the width of the cuvette, i.e., 1 cm), and $C$ is the concentration of the $KP_{15}$ dispersions. The absorbance $A$ and the absorption coefficient $K$ are related to the wavelength of the incident light. To determine $A$ and $K$, it is necessary to choose a specific incident wavelength. The bandgap of bulk $KP_{15}$ is approx. 1.75 eV [20]. However, according to our previous study, with thickness reduction of the $KP_{15}$ nanowires, a surface-state luminescence at 693 nm gradually dominates in the $KP_{15}$ nanowire [14]. This could affect light absorption properties of $KP_{15}$ due to its decreased size.

To avoid the generation of concentration error caused by the absorbance influence of the surface state, a wavelength (800 nm) which is far away from the bandgap of $KP_{15}$ bulk and surface state in the $KP_{15}$ nanowires was chosen. Some dispersions for which we predetermined the concentration were prepared to fit and determine the absorption coefficient $K$. Solutions of five different concentrations of $KP_{15}$ dispersions in butyrolactone were prepared by liquid exfoliation with a predetermined concentration. UV−visible absorption spectra results are shown in Figure 2. The concentration linearly varies with absorbance. The slope of this fitted linear equation is 3.86 ± 0.13. This means that the absorption coefficient of $KP_{15}$ is 3.86 ± 0.13 $mL \cdot mg^{-1} \cdot cm^{-1}$.

We selected 20 common solvents, including benzyl benzoate, toluene, ethyl acetate, acetone, alcohol, butyrolactone, *N*,*N*'-dimethylpropyleneurea, bromobenzene, cyclopentanone, *N*-dodecyl-2-pyrrolidone, glycol, vinyl acetate, hexane, isopropyl alcohol, *N*,*N*-dimethylformamide, *O*-phthalic dimethyl ester, dimethyl sulfoxide, *N*-methylpyrrolidone, water, and cyclohexanone. The HSPs of those solvents are listed in Table 1.

Figure 3 exhibits the concentrations of $KP_{15}$ dispersions exfoliated in different solvents. Cyclopentanone and butyrolactone were more suitable than the other solvents to exfoliate $KP_{15}$. Figure 4 shows the relationship between the HSPs of different solvents and the concentration of the $KP_{15}$ suspension. Based on Equation 2, the HSPs of $KP_{15}$ were $\delta_D$ = 17.60 $MPa^{1/2}$,

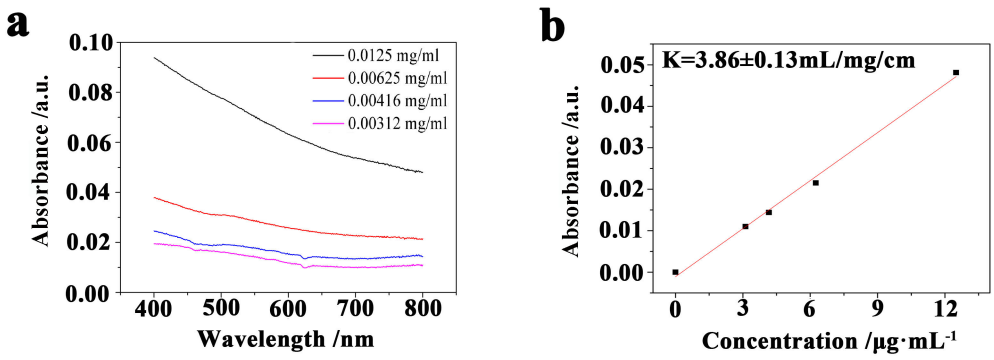


**Figure 2:** Absorbance of predetermined $KP_{15}$ dispersions exfoliated in butyrolactone. (a) Absorbance of different concentrations of predetermined $KP_{15}$ dispersions exfoliated in butyrolactone. (b) Absorbance (800 nm) as a function of concentration of predetermined $KP_{15}$ dispersions. The absorption coefficient (800 nm) is 3.86 ± 0.13 mL·mg$^{-1}$·cm$^{-1}$.

**Table 1:** Hansen parameters for the solvents [21].

| solvent | $\delta_D$ (MPa$^{1/2}$) | $\delta_P$ (MPa$^{1/2}$) | $\delta_H$ (MPa$^{1/2}$) |
|---|---|---|---|
| benzyl benzoate | 20 | 5.1 | 5.2 |
| toluene | 18 | 1.4 | 2 |
| ethyl acetate | 15.8 | 5.3 | 7.2 |
| acetone | 15.5 | 10.4 | 7 |
| alcohol | 18.1 | 17.1 | 16.9 |
| butyrolactone | 18 | 16.6 | 7.4 |
| *N*,*N*'-dimethylpropyleneurea | 17.8 | 9.5 | 9.3 |
| bromobenzene | 19.2 | 5.5 | 4.1 |
| cyclopentanone | 17.9 | 11.9 | 5.2 |
| *N*-dodecyl-2-pyrrolidone | 17.5 | 4.1 | 3.2 |
| glycol | 17 | 11 | 26 |
| vinyl acetate | 16 | 7.2 | 5.9 |
| hexane | 14.9 | 0 | 0 |
| isopropyl alcohol | 15.8 | 6.1 | 16.4 |
| *N*,*N*-dimethylformamide | 17.4 | 13.7 | 11.3 |
| *O*-phthalic dimethyl ester | 18.6 | 10.8 | 4.9 |
| dimethyl sulfoxide | 18.4 | 16.4 | 10.2 |
| *N*-methylpyrrolidone | 18 | 12.3 | 7.2 |
| water | 15.8 | 8.8 | 19.4 |
| cyclohexanone | 17.8 | 8.4 | 5.1 |

$\delta_P$ = 11.19 MPa$^{1/2}$, and $\delta_H$ = 8.95 MPa$^{1/2}$. As long as the difference between the HSPs of $KP_{15}$ and the HSPs of a given solvent is reduced, τ can be reduced with an improved exfoliation efficiency. Figure 5 shows the concentration of $KP_{15}$ dispersions as a function of τ. When τ tends to zero, the concentration of the $KP_{15}$ dispersion reaches the maximum value, which corresponds to the results of the aforementioned equation.

## Liquid exfoliation of one-dimensional $KP_{15}$

The HSPs obtained for $KP_{15}$ were $\delta_D$ = 17.60 MPa$^{1/2}$, $\delta_P$ = 11.19 MPa$^{1/2}$, and $\delta_H$ = 8.95 MPa$^{1/2}$. We chose a mixed solution containing water and acetone to exfoliate $KP_{15}$. The HSPs of water were $\delta_D$ = 15.8 MPa$^{1/2}$, $\delta_P$ = 8.8 MPa$^{1/2}$, and $\delta_H$ = 19.4 MPa$^{1/2}$. The HSPs of acetone were $\delta_D$ = 15.5 MPa$^{1/2}$, $\delta_P$ = 10.4 MPa$^{1/2}$, and $\delta_H$ = 7.0 MPa$^{1/2}$. The HSP range of a mixed solution of water and acetone can cover the HSPs of $KP_{15}$, however, both of them can be easily removed. The HSPs ($\delta_i$) in a mixed solution containing water and acetone can be expressed by Equation 4.

$$\delta_i = \sum \phi_{i,\text{comp}} \delta_{i,\text{comp}}, \quad (4)$$

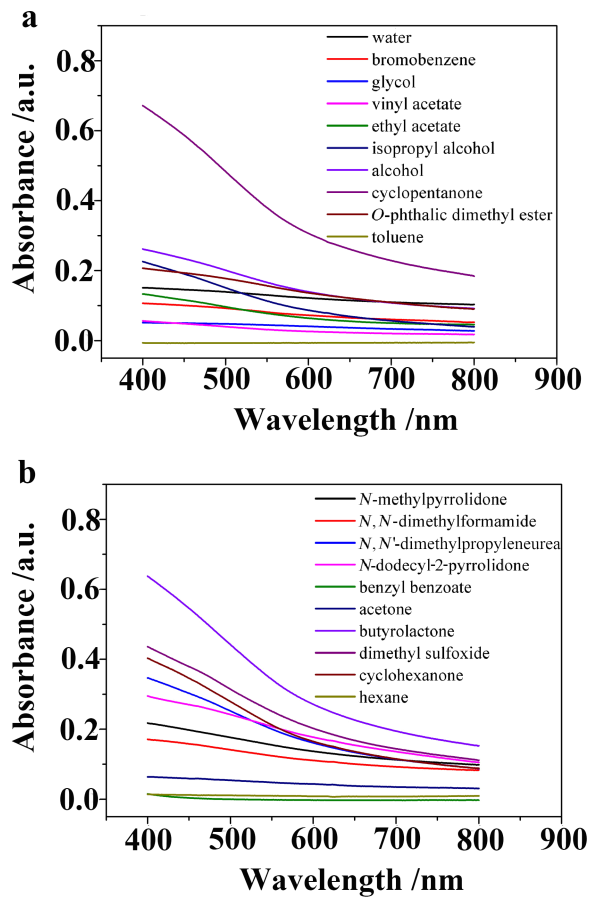


**Figure 3:** UV–visible spectrum of the $KP_{15}$ dispersions using various solvents.

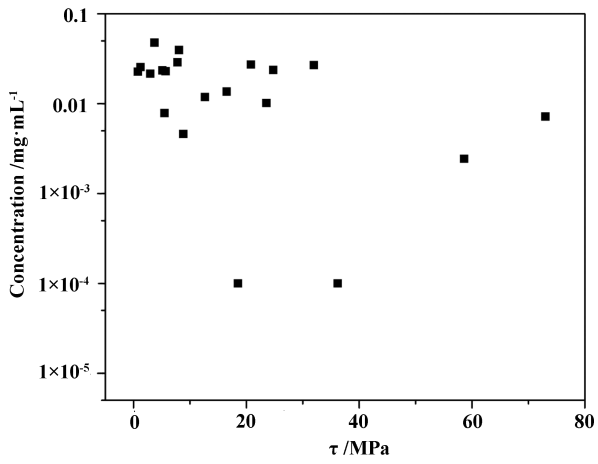


**Figure 5:** Concentration of $KP_{15}$ dispersions as a function of τ, $\tau = [(\delta_{A,D} - \delta_{B,D})^2 + (\delta_{A,P} - \delta_{B,P})^2/4 + (\delta_{A,H} - \delta_{B,H})^2/4]$.

where $\phi_{i,comp}$ is the volume fraction of the corresponding solvent and $\delta_{i,comp}$ is the HSPs of the solvent. The concentration of the $KP_{15}$ dispersion can be measured by the Lambert–Beer law (Equation 3). As shown in Figure 6a, by tuning the volume fraction of acetone in the mixed solution, the HSPs of the mixed solution can be close to those of $KP_{15}$, and the exfoliation efficiency can be clearly improved. The concentration values of the $KP_{15}$ suspension in the solutions were 0.0268 mg·mL$^{-1}$ (exfoliated in deionized water), 0.0079 mg·mL$^{-1}$ (acetone), and 0.0236 mg·mL$^{-1}$ (alcohol), respectively [13]. When the solvent mixture with a 50% volume fraction of acetone is used for stripping, the concentration of the $KP_{15}$ dispersion finally increases to 0.0458 mg·mL$^{-1}$. At this point, the parameter τ is close to the minimum value.

The Raman result for the $KP_{15}$ nanowires exfoliated in water–acetone mixed solution is shown in Figure 7c. At least 11 distinguishable Raman peaks located at 476.6, 453.0, 408.8, 378.3, 368.4, 354.1, 303.7, 288.5, 126.1, 114.1, and 90.7 cm$^{-1}$ were seen and those Raman results were similar to the Raman modes of mechanically exfoliated $KP_{15}$ [11]. As shown in Figure 7d, Figure 7e, and Figure 8, the thinnest $KP_{15}$ nanowires obtained by liquid exfoliation could reach 5.1 nm and had smooth boundaries. The thicknesses of 79% of the liquid-exfoli-

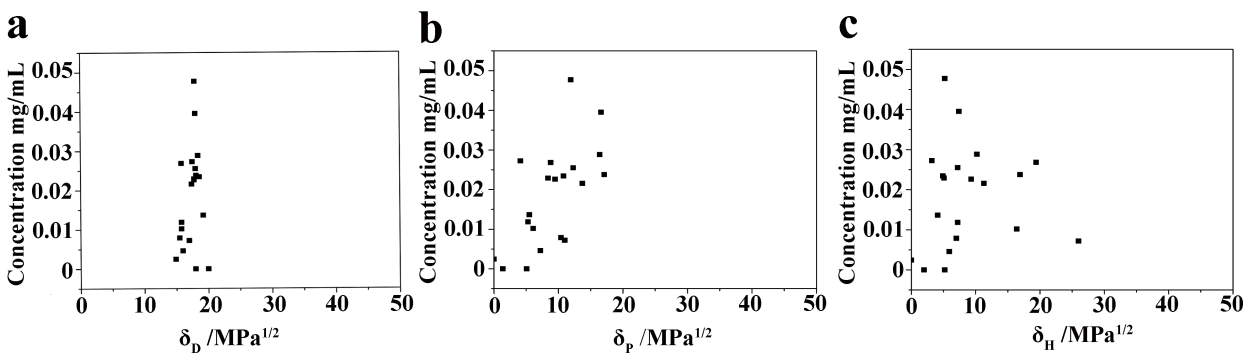


**Figure 4:** Concentration of $KP_{15}$ dispersions as a function of the Hansen parameters. (a) Concentration of $KP_{15}$ dispersions as a function of $\delta_D$. (b) Concentration of $KP_{15}$ dispersions as a function of $\delta_P$. (c) Concentration of $KP_{15}$ dispersions as a function of $\delta_H$.

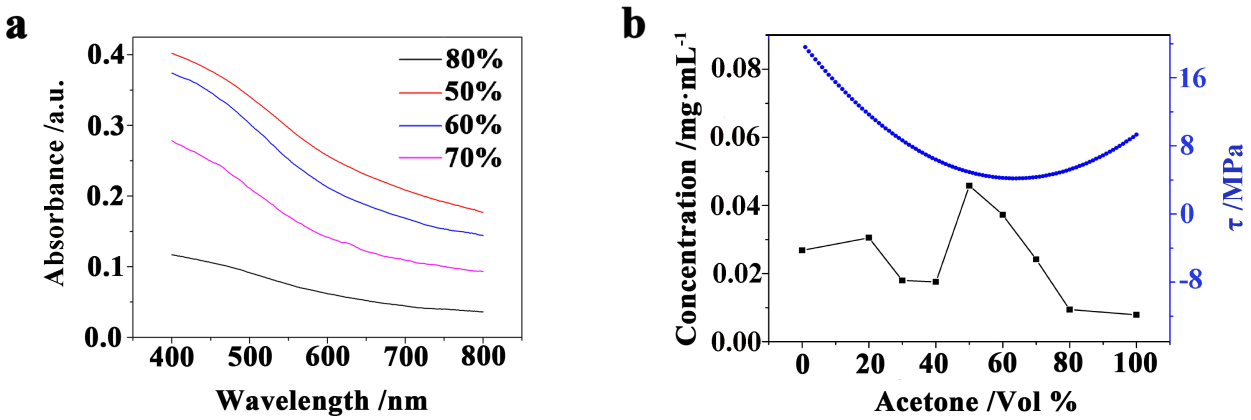


**Figure 6:** Results of $KP_{15}$ dispersions exfoliated in acetone/water mixtures. (a) Absorbance of $KP_{15}$ dispersions exfoliated in acetone/water mixtures with different acetone volume fractions. (b) $KP_{15}$ suspension concentration and the calculated τ as a function of the acetone volume fraction.

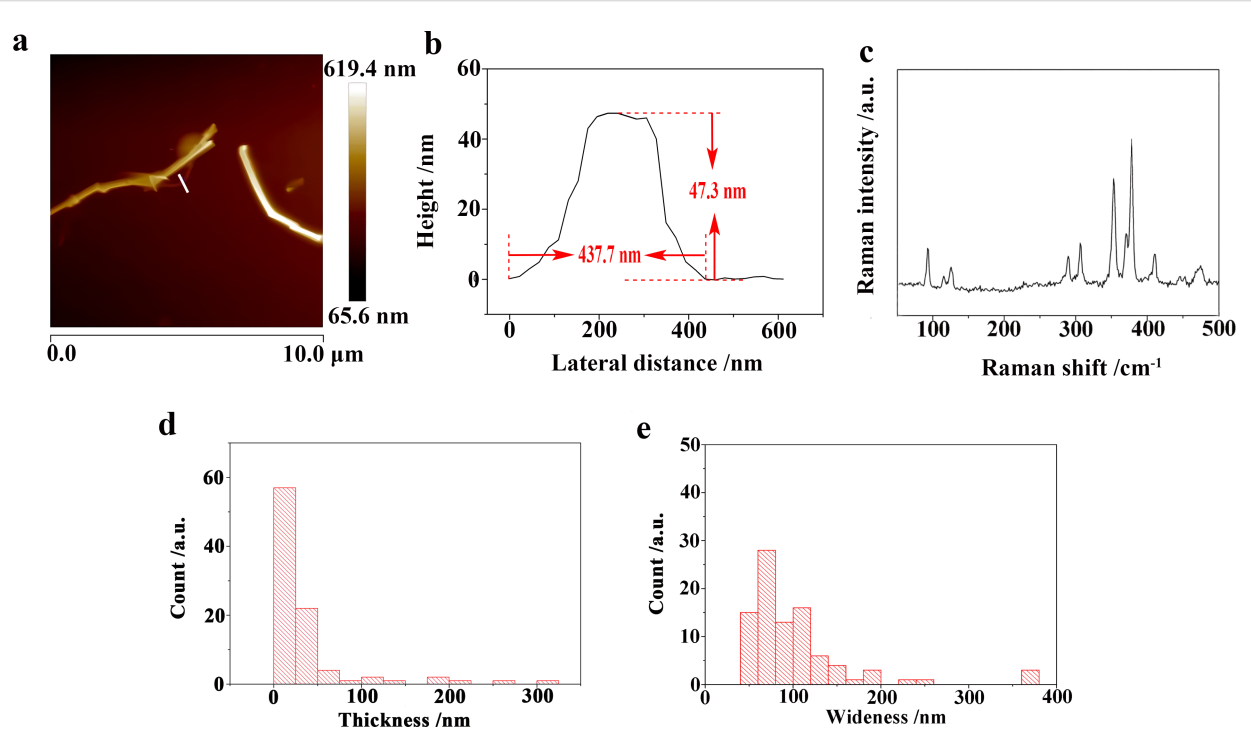


**Figure 7:** (a) Height distribution of $KP_{15}$ nanowires after liquid exfoliation. (b) Cross sections of $KP_{15}$ nanowires after liquid exfoliation. (c) Raman spectra of $KP_{15}$ nanowires after liquid exfoliation. (d) Thickness histograms of $KP_{15}$ nanowires after liquid exfoliation. (e) Width histograms of $KP_{15}$ nanowires after liquid exfoliation.

ated $KP_{15}$ nanowires were below 50 nm; the widths of 60.9% of the $KP_{15}$ nanowires were below 100 nm. The sizes of the obtained $KP_{15}$ nanowires were much smaller than those obtained in our previous studies [13]. Meanwhile, a strong temperature-dependent Raman response in exfoliated $KP_{15}$ nanowires has been observed. That may help with non-invasive temperature measurements of $KP_{15}$ nanodevices (details are demonstrated in Supporting Information File 1).

## Conclusion

In summary, based on the Hansen's empirical theory, the liquid phase exfoliation efficiency of $KP_{15}$ nanowires has been improved. The HSPs of $KP_{15}$ were calculated to be $\delta_D$ = 17.60 $MPa^{1/2}$, $\delta_P$ = 11.19 $MPa^{1/2}$, and $\delta_H$ = 8.95 $MPa^{1/2}$. In addition, based on the Hansen's empirical theory, the exfoliation efficiency was improved by adjusting the ratio of water and acetone. When the mixed solvents had the smallest τ, the thick-

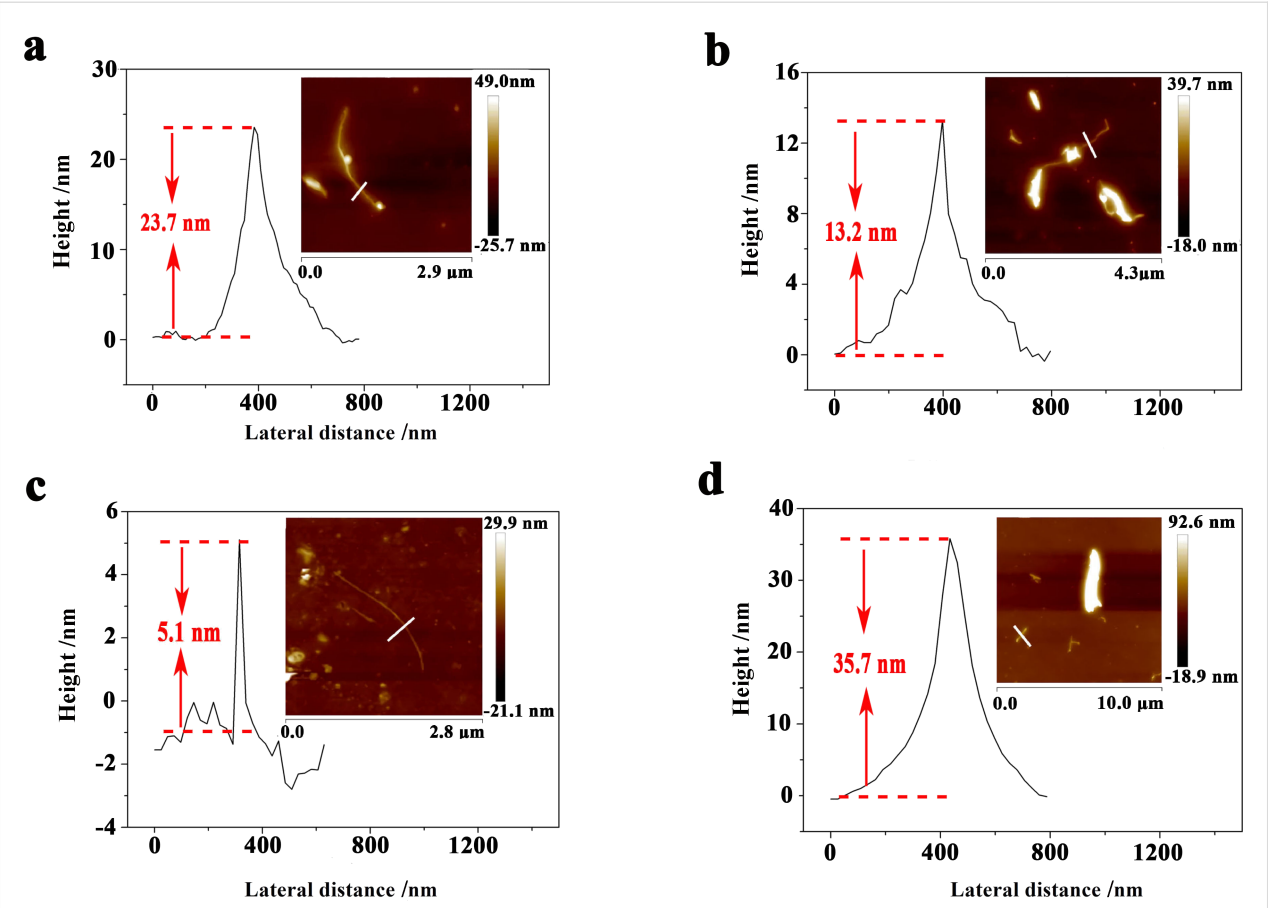


**Figure 8:** Sizes of exfoliated $KP_{15}$ nanowires. (a) Cross section of the $KP_{15}$ nanowire marked in the upper right corner inset image. (b) Cross section of the $KP_{15}$ nanowire marked in the upper right corner inset image. (c) Cross section of the $KP_{15}$ nanowire marked in the upper right corner inset image. (d) Cross section of the $KP_{15}$ nanowire marked in the upper right corner inset image.

nesses of 79% of liquid-exfoliated $KP_{15}$ nanowires were below 50 nm and the widths of 60.9% of $KP_{15}$ nanowires were below 100 nm. Meanwhile, a strong temperature-dependent Raman response has been found in exfoliated $KP_{15}$, which may help with non-invasive temperature measurements of $KP_{15}$ nanodevices.

## Supporting Information

### Supporting Information File 1

Strong temperature-dependent Raman response of exfoliated $KP_{15}$.
[https://www.beilstein-journals.org/bjnano/content/supplementary/2190-4286-13-69-S1.pdf]

## Funding

This work was supported by the National Natural Science Foundation of China under the grant (51972006), Guangxi Key Laboratory of Optical and Electronic Materials and Devices (20AA-19), Guilin University of Technology research fund (GUTQDJJ2019031), Guangxi Young and middle-aged teachers' basic ability improvement project (2021KY0251), National Natural Science Foundation of China (U20A20245), Guangxi Distinguished Experts Special Fund (2019B06), Guangxi Research Foundation for Science and Technology Base and Talent Special (AD19245175), National Natural Science Foundation of China (NFSC) (52002318), and National Science Foundation of Shaanxi Province (2020JQ-841).

## ORCID® iDs

Nan Tian - https://orcid.org/0000-0002-1423-7581
Danmin Liu - https://orcid.org/0000-0002-4031-1351

## References

1. Yang, B.; Chen, J.; Liu, B.; Ding, Y.; Tang, Y.; Yan, X. *J. Mater. Chem. A* **2021,** *9,* 6352–6360. doi:10.1039/d1ta00404b
2. Zhao, R.; Wei, Q.; Ran, Y.; Kong, Y.; Ma, D.; Su, L.; Yao, L.; Wang, Y. *Nanotechnology* **2021,** *32,* 375501. doi:10.1088/1361-6528/ac06f6

3. Fei, B.; Chen, C.; Hu, C.; Cai, D.; Wang, Q.; Zhan, H. *ACS Appl. Energy Mater.* **2020,** *3,* 9018–9027. doi:10.1021/acsaem.0c01431
4. Jiang, X.; Qin, S.; Cao, Y.; Wu, R.; Han, D.; Hua, Z.; Zhu, C.; Huang, X.; Wang, L.; Yang, S. *ACS Appl. Nano Mater.* **2020,** *3,* 3402–3409. doi:10.1021/acsanm.0c00152
5. Island, J. O.; Buscema, M.; Barawi, M.; Clamagirand, J. M.; Ares, J. R.; Sánchez, C.; Ferrer, I. J.; Steele, G. A.; van der Zant, H. S. J.; Castellanos-Gomez, A. *Adv. Opt. Mater.* **2014,** *2,* 641–645. doi:10.1002/adom.201400043
6. Dai, J.; Zeng, X. C. *Angew. Chem.* **2015,** *127,* 7682–7686. doi:10.1002/ange.201502107
7. Island, J. O.; Barawi, M.; Biele, R.; Almazán, A.; Clamagirand, J. M.; Ares, J. R.; Sánchez, C.; van der Zant, H. S. J.; Álvarez, J. V.; D'Agosta, R.; Ferrer, I. J.; Castellanos-Gomez, A. *Adv. Mater. (Weinheim, Ger.)* **2015,** *27,* 2595–2601. doi:10.1002/adma.201405632
8. Eckstein, N.; Hohmann, A.; Weihrich, R.; Nilges, T.; Schmidt, P. *Z. Anorg. Allg. Chem.* **2013,** *639,* 2741–2743. doi:10.1002/zaac.201300327
9. Zhang, G.; Liu, D.; Tian, N.; Liu, B.; Li, S.; You, C.; Qu, X.; Ma, H.; Fan, C.; Zhang, Y. *Inorg. Chem.* **2020,** *59,* 976–979. doi:10.1021/acs.inorgchem.9b03188
10. Smith, J. B.; Hagaman, D.; DiGuiseppi, D.; Schweitzer-Stenner, R.; Ji, H.-F. *Angew. Chem., Int. Ed.* **2016,** *55,* 11829–11833. doi:10.1002/anie.201605516
11. Tian, N.; Yang, Y.; Liu, D.; Liu, X.; Tan, P.-H.; Zhang, D.; Chang, K.; Li, H.; Zhao, M.; Li, J. R.; Tang, X.; Zhang, D.; Zhang, Z.; Xiao, W.; Yan, H.; Zhang, Y. *ACS Nano* **2018,** *12,* 1712–1719. doi:10.1021/acsnano.7b08368
12. Yang, Y.; Chen, X.; Tian, N.; Zhang, Y.; Liu, D.; Yan, H. *Mater. Lett.* **2020,** *272,* 127826. doi:10.1016/j.matlet.2020.127826
13. Tian, N.; Liu, D.; Zhou, B.; Yang, Y.; Zhang, G.; Zhang, D.; Zhang, Y. *Mater. Lett.* **2018,** *228,* 89–91. doi:10.1016/j.matlet.2018.05.048
14. Tian, N.; Liu, D.; Yang, Y.; Zhang, G.; Zhang, D.; Zhang, Y. *Nanoscale* **2018,** *10,* 16479–16484. doi:10.1039/c8nr05766d
15. Alzakia, F. I.; Tan, S. C. *Adv. Sci.* **2021,** *8,* 2003864. doi:10.1002/advs.202003864
16. Qin, J.; Wang, X.; Jiang, Q.; Cao, M. *ChemPhysChem* **2019,** *20,* 1069–1097. doi:10.1002/cphc.201900110
17. Xie, Y.-M.; Yao, Q.; Xue, Q.; Zeng, Z.; Niu, T.; Zhou, Y.; Zhuo, M.-P.; Tsang, S.-W.; Yip, H.-L.; Cao, Y. *Interdiscip. Mater.* **2022,** *1,* 281–293. doi:10.1002/idm2.12023
18. Zhang, G.; Liu, D.; Tian, N.; Wang, X.; Yan, W.; Huang, Z.; Zhang, Y. *Inorg. Chem.* **2021,** *60,* 4883–4890. doi:10.1021/acs.inorgchem.0c03791
19. Hernandez, Y.; Lotya, M.; Rickard, D.; Bergin, S. D.; Coleman, J. N. *Langmuir* **2010,** *26,* 3208–3213. doi:10.1021/la903188a
20. Olego, D. J. *Phys. Rev. B* **1985,** *31,* 2230–2239. doi:10.1103/physrevb.31.2230
21. Barton, A. F. M. *CRC handbook of solubility parameters and other cohesion parameters;* CRC Press: Boca Raton, FL, USA, 1991.

## License and Terms